

Ventilated oscillatory boundary layers

By DANIEL C. CONLEY† AND DOUGLAS L. INMAN

Center for Coastal Studies, Scripps Institution of Oceanography, University of California at San Diego, La Jolla, CA 92093-0209, USA

(Received 15 June 1993 and in revised form 25 February 1994)

Boundary layers arising from flows which oscillate parallel to a permeable bed, and are subject to oscillating percolation of the same frequency as the bed parallel flow, referred to here as ‘ventilated oscillatory boundary layers’, are the subject of this laboratory study. These boundary layers are intended to approximate naturally occurring wave boundary layers over permeable beds. Measurements of boundary-layer velocities, bed stress and turbulent flow properties are presented. It is observed that suction (flow into the bed) enhances the near-bed velocities and bed stress while injection (flow out of the bed) leads to a reduction in these quantities. As the ventilated oscillatory boundary layer experiences both these phenomenon in one full cycle, the result is a net stress and a net boundary-layer velocity in an otherwise symmetric flow. While production of turbulence attributable to injection is enhanced, the finite time required for this to occur leads to a greater vertically averaged turbulence in the suction half-cycle. Turbulence generated in the suction half-cycle is maintained in a compact layer much closer to the bed. These effects appear to hold for Re ranging from 10^5 to 10^6 and for oscillations other than sinusoidal.

1. Introduction

Laboratory studies of the boundary layer arising from oscillatory flow have always treated the problem as a cyclical process composed of two purely symmetrical half-cycles (e.g. Jonsson 1963; Sleath 1987). Asymmetries occurring in the laboratory (Flick, Guza & Inman 1981) or the field (Hanes & Huntley 1986) have been explained by asymmetries in the fluid velocity or acceleration inherent in shoaling waves. In a paper reporting on field observations of wave-driven oscillatory boundary layers over sand beds, Conley & Inman (1992) reported the observation of an asymmetry in the development of the boundary layer which could not be explained by velocity or acceleration asymmetries in the overlying fluid. As an explanation for this asymmetry, they proposed a type of transpired boundary layer which is here called the ventilated oscillatory boundary layer. This work reports on laboratory experiments designed to investigate the effect of boundary ventilation on the velocities, bed stress and turbulent flow properties of the turbulent oscillatory boundary layer.

Boundary layers which arise from a fluid flowing with velocity u parallel to a solid permeable boundary through which a secondary fluid is flowing with boundary-normal velocity w have practical significance in many applications (e.g. drag reduction, boundary-layer control) and have been the subject of studies for well over forty years (e.g. Libby, Kaufman & Harrington 1952; Antonia *et al.* 1990). These boundary layers

† Present address: Marine Sciences Research Center, State University of New York, Stony Brook, NY 11794-5000, USA.

are generally known as transpired boundary layers and the secondary flow through the boundary is generally referred to as transpiration (Kays 1972). If the transpiration is from the boundary into the overlying fluid ($w > 0$), it is called injection or blowing. If the flow is from the fluid into the boundary ($w < 0$), it is termed suction. In general the two fluids are identical and the transpired flow is smaller in magnitude than the boundary-parallel flow so that the transpiration parameter $V = w/u$ has a magnitude less than 1.

Ventilated oscillatory boundary layer is a term applied here to the boundary layer arising from an oscillating boundary-parallel flow subject to oscillating transpiration of the same period and shape. In most of this work, the boundary-parallel flow is of the form $u(t) = u_m \sin(\sigma t)$ and subject to transpiration of the form $w(t) = w_m \sin(\sigma t + \phi)$. Here $\sigma = 2\pi/T$ is the radian frequency, T is the period and ϕ is an arbitrary constant phase. Analogous to the transpiration parameter V , we shall define a flow ventilation parameter \tilde{V} as $|\tilde{V}| = w_m/u_m$. The sign of \tilde{V} indicates whether injection ($\tilde{V} > 0$) or suction ($\tilde{V} < 0$) occurs concurrently with positive flow. Additionally, we define an instantaneous ventilation parameter $\tilde{V}' = w(t)/u(t)$. Through most of this work, the phase ϕ will be 0 in which case \tilde{V}' becomes a constant, identically equal to \tilde{V} .

In general, boundary transpiration affects the boundary-layer velocity profile. Suction tends to pull streamlines down closer to the bed shifting the velocity profile closer to the bed. This results in higher shear near the bed and therefore higher shear stress at the bed. This is demonstrated quite clearly in a comparison of the asymptotic suction profile (an exact solution to the Navier–Stokes equations for laminar flow over a flat plate with constant suction) and the Blasius profile (Schlichting 1979). In contrast, injection results in a spreading of the streamlines near the boundary which reduces the near-bed shear and the resultant bed stress.

In a study of turbulent boundary layers in steady flow over flat plates with injection, Mickley & Davis (1957) showed that the friction factor C_f is a strong function of V and Re_x , where Re_x is the Reynolds number based on distance along the plate. However, their results can be shown to indicate that the ratio C_f/C_{f_0} , where C_{f_0} is the friction factor without injection, is a strong function of V but exhibits almost no Re_x dependency. The results of Simpson, Moffat & Kays (1969) show the same to be true for steady suction on a flat plate. In a rough analysis based on film theory, Mickley *et al.* (1954) showed that this ratio should depend on the ventilation parameter as

$$\frac{C_f}{C_{f_0}} = \frac{bV/C_{f_0}}{e^{bV/C_{f_0}} - 1}, \quad (1)$$

where b is a constant equal to 2 in theory.

The asymptotic suction profile shows reduced curvature in the boundary-layer velocity profile relative to the Blasius profile (Schlichting 1979). This suggests that suction tends to stabilize the flow. Analytical solutions for boundary layers with injection show an inflexion point in the velocity profile suggesting that injection tends to destabilize the flow. Experiments have shown these findings to be true not only for laminar flow but for turbulent flow as well. Tewfik (1963) demonstrated that turbulent boundary layers with injection were thicker than would be the case without injection. It was also shown that whereas injection reduces stress at the bed and throughout the inner tenth of the boundary layer, it increased it elsewhere. Antonia *et al.* (1988) reconfirmed that suction results in a significant reduction in turbulent velocity fluctuations u' and w' . While investigating the effect of suction on organized motion in

turbulent boundary layers, they observed that low-speed streaks in the near-wall region were more persistent and that the frequency of dye injections into the outer layer was reduced. This is consistent with the results of Fulachier *et al.* (1982) where the rate of turbulent production was found to decrease and the relative contribution of large-scale structures was found to increase.

Kays (1972) shows that turbulent boundary layers under injection seem to respond to prevailing conditions. In particular, a boundary layer experiencing a sudden increase in injection will, following a short period of adjustment, behave as though it had always been subject to that level of injection. This appears to be less true for a reduction in injection where the flow appeared to retain a 'memory' of the earlier higher level of injection. It is also shown that transpired boundary layers are sensitive to acceleration, the sensitivity increasing with V . These studies raise questions as to how a ventilated oscillatory boundary layer will behave as such boundary layers are constantly subject to acceleration and changing conditions. In a study designed to examine the effect of transpiration on sediment transport, Lofquist (1975) found that sand ripples in a ventilated oscillatory flow preferentially migrated in the direction of flow subject to suction. This was assumed to indicate that bed stress was greater during suction than during injection, but no studies which examine the quantitative effects of transpiration on the flow in oscillatory conditions have been reported.

2. Experimental set-up

The experiments have been performed in water using the oscillatory flow tunnel (OFT) at the Scripps Institution of Oceanography hydraulics laboratory (figure 1). The OFT is composed of an acrylic working section 14.0 m long which terminates in painted steel cylindrical risers at each end. One riser acts as a reservoir and is open to the atmosphere; the other riser is sealed by a 62 cm diameter acrylic piston which drives the oscillating flow. The piston is driven by a hydraulic ram which is controlled via a servo amplifier that responds to any arbitrary electrical input. Further details of the facility are described by King, Powell & Seymour (1984). For these experiments a false floor was placed in the working section giving a tunnel cross-section 39 cm wide and 28 cm deep. The test section was created by placing a rigid permeable floor in the centre 4.25 m of the working section. This floor was formed from fourteen 30×30 cm bricks of fused Alundum which were 2.5 cm thick. These bricks were composed of Alundum grains with a mean diameter of $250 \mu\text{m}$ which were fused under high temperature. Prior to firing, the bricks were pressed at high pressure. As a result, flat surfaces of the rather angular grains aligned to form a smooth surface on the bricks. Any roughness in the bed was due to pores in the surface, not protuberant grains. The mean pore size of the internal pores is stated to be $180 \mu\text{m}$. A secondary piston which was plumbed into the cavity below the test section was used to drive the boundary-layer ventilation.

Tests were performed using a period of oscillation $T = 7$ s and an orbital displacement d_0 of 207 cm. This resulted in a flow with oscillatory Reynolds number \overline{Re} of 1.0×10^6 . \overline{Re} is defined as

$$\overline{Re} = u_m d_0 / 2\nu, \quad (2)$$

where u_m is the maximum mass-averaged velocity. The results of Jensen, Sumer & Fredsoe (1989) have shown that oscillatory boundary layers of this \overline{Re} will be fully turbulent for phases greater than 45° and transitional for phases greater than 15° , where zero phase corresponds to zero velocity. The oscillatory period used in this study

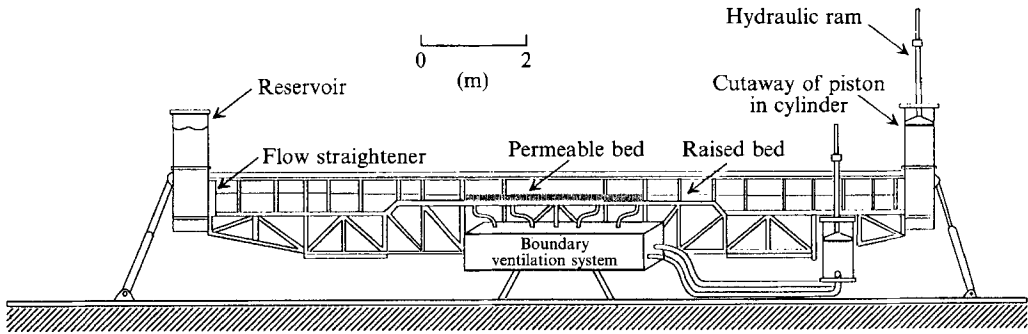


FIGURE 1. Schematic of the oscillatory flow tunnel showing permeable test bed and boundary ventilation pumping system.

was selected to be as large as possible and still produce an \widetilde{Re} of this magnitude. For the unventilated case, the boundary-layer thickness δ_0 is 1.8 cm, where δ_0 has been defined as the first level at which the vertical derivative of velocity vanishes at a phase of 90° . The maximum friction velocity $u_{*m} = (\tau_m/\rho)^{1/2}$ is 4.1 cm s^{-1} . The bed was determined to be hydraulically smooth. The ventilation parameter \widetilde{V} was zero in the control tests and ranged in magnitude from 8.2×10^{-4} to 1.3×10^{-2} in other tests. The amplitude of w was calculated by assuming uniform velocity over the test bed and distributing the volumetric displacement of the secondary piston over the entire test bed. Calculations indicated that uniform velocity over the test bed was a good assumption given the manufacturers supplied permeability of 192 Darcys for the Alundum bricks. This assumption was tested through dye studies in which no systematic variations in the flow through the bricks could be detected.

Three main quantities are presented in this work: the bed stress $\tau(t)$, fluid velocity $u(z, t)$ and the vertical component of fluctuating velocity $w'(z, t)$. The bed shear stress was measured using a TSI model 1237 W flush-mounted hot-film sensor as shown in figure 2. The sensor was locked into an acrylic probe holder 9.5 mm in diameter which fitted through an O-ring seal into a cylindrical acrylic sleeve with a wall thickness of 1.8 mm. The sleeve was permanently epoxied into the test bed with the top of the sleeve flush with the surface of the Alundum bed. When inserted, the tops of the probe and holder were level with the top of the sleeve. This arrangement allowed the shear stress sensor to be calibrated in a separate facility and to maintain the same orientation between probe and holder when transferred to the test facility. It should be noted that the presence of the solid probe and holder prevents application of ventilation directly at the point of measurement. This implies that the measured bed stresses are representative of sections of the bed which do not experience the full effect of ventilation and that the measurements represent an underestimate of the full effects of ventilation. None the less this effect is expected to be minimal as the ratio of diameter of the probe holder to orbital displacement is $O(10^{-2})$.

The longitudinal component of velocity was measured using a TSI model 1210-20 W cylindrical hot-film sensor. The probe was mounted on a sting projecting through the lid of the OFT with the axis of the sensing element horizontal and transverse to the direction of flow. This probe was calibrated by placing it in the tunnel centre and calibrating against the tunnel mass-averaged velocity using a technique adopted from Flick & George (1990). Since the hot film measures fluid speed, the time series was derectified using the mass-averaged fluid velocity as a zero-crossing reference. Turbulent velocity fluctuations were measured using a TSI model 1287 W split film hot

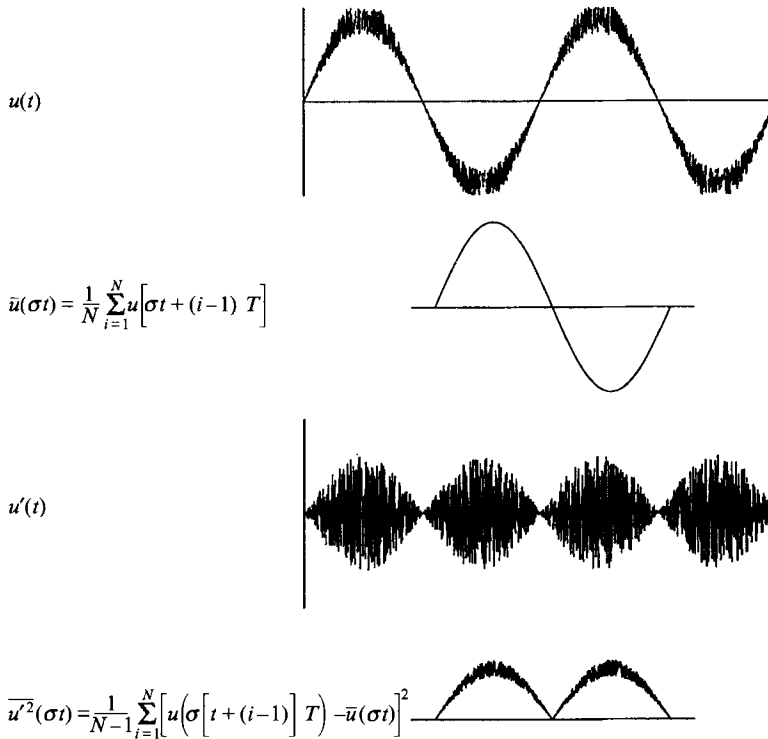


FIGURE 3. Schematic representation of the turbulent decomposition of an oscillating quantity.

rotation of the support about its fixed location at the tunnel lid. Geometrical arguments indicate that the signal contamination in the vertical would be less than 1% of the minimum measured signal. When compared to the results of other investigators, these arguments seem to be valid and the results for w' appear to be unaffected by the vibrations. This difficulty explains why no results for u' or $\overline{u'w'}$ are presented.

Depending on the test, data runs were of 500 or 700 s in duration. The time series collected over each run were ensemble averaged in order to determine the phase-averaged quantities. In oscillatory flows, the turbulent decomposition of a flow property $\xi(t)$ has three components: the time mean $\langle \xi \rangle$, the ensemble-averaged mean $\bar{\xi}(\theta)$ and the ensemble-averaged r.m.s. mean of the fluctuating quantity $\bar{\xi}'(\theta)$. In these relations, θ represents the phase of an ensemble-averaged quantity, and it is understood to range from 0° to 360° . In a purely oscillatory flow, the traditionally defined time mean is identically zero. For a time series collected over N cycles of period T , the ensemble-averaged mean is calculated as

$$\bar{\xi}(\sigma t) = \frac{1}{N} \sum_{i=1}^N \xi(\sigma t + (i-1)T), \quad (3)$$

where $\sigma = 2\pi/T$ is the radian frequency. This definition is valid for $t = 0$ to T in keeping with the above-mentioned convention relating to the phase of ensemble-averaged quantities. Similarly the ensemble-averaged r.m.s. mean of the fluctuating quantity is defined by

$$\bar{\xi}'(\sigma t) = \left\{ \frac{1}{N-1} \sum_{i=1}^N [\xi(\sigma t + (i-1)T) - \bar{\xi}(\sigma t)]^2 \right\}^{1/2}. \quad (4)$$

This decomposition shown schematically in figure 3. Sleath (1987) and others have shown that there is no significant improvement in the consistency of the estimate of ensemble-averaged mean quantities for averages of greater than 50 cycles. The results from the 500 s tests in this work were averaged over 71 cycles and the results for the 700 s tests were averaged over 100 cycles. The convention that the phase $\theta = 0$ corresponds to the negative-to-positive velocity zero crossing in the oscillatory flow will be used.

3. Effects of ventilation

The ensemble-averaged centreline velocity for the case of no flow through the bed is shown in figure 4(a). As can be seen from the plot, the velocity is relatively symmetric throughout the entire cycle. Each half-cycle appears qualitatively similar to the other half-cycle and the accelerating portions of each half-cycle appear to be mirror images of the decelerating portions. Figure 4(b) is a plot of ensemble-averaged centreline acceleration as calculated by differentiating the smoothed velocity signal in figure 4(a). This plot reveals asymmetries in the flow which are not obvious in the velocity. In particular it is seen that acceleration tends towards a monotonical decrease throughout the first half-cycle as would be expected in an oscillatory flow. This is not true for the second half-cycle where periods of decreasing acceleration are clearly present in what would be expected to be a time of monotonically increasing acceleration. Study of the apparatus indicated that these fluctuations represent an instability in the hydraulic ram during the midstroke transition from compressive to extensive loading. This instability is seen by the fluid as a small fluctuation in the forcing pressure gradient.

While these fluctuations do not have a readily apparent effect on fluid velocity it might be anticipated that the fluctuations in pressure gradient would have a larger effect in the boundary layer and on the bed stress. This seems to be borne out by the results presented in figure 4(c). The solid line represents the ensemble-averaged bed stress as derived from the shear-stress sensor. The bed stress in the second half-cycle is much peakier than would be expected in an oscillatory flow of this Reynolds number, $Re = 10^6$, whereas the first half-cycle is more typical (see Jensen *et al.* 1989).

Jensen *et al.* (1989) have shown that the boundary-layer velocity profiles in high-Reynolds-number flows do exhibit a logarithmic layer, at least during periods of low pressure gradient. The velocity profile in this layer follows the traditional 'law of the wall' behaviour where

$$u^+ = 5.5 + \frac{1}{\kappa} \ln z^+, \quad (5)$$

where $u^+ = u/u_*$ and $z^+ = zu_*/\nu$ are the non-dimensional 'wall variables', $\kappa = 0.4$ is von Kármán's constant and $u_* = (\tau_0/\rho)^{1/2}$ is the friction velocity. In order to test this in the present experiments, bed stress was taken as the average value derived from applying (5) to the velocities in the log layer. For this calculation, the log layer was defined to extend from $z^+ = 13$ to 130, where z^+ was calculated using u_{*m} . The values of bed stress so calculated are plotted as heavy dots in figure 4(c). This technique gives a reasonable estimate of bed stress in the first half-cycle with some overprediction. However, when this same procedure is performed on the second half-cycle, it results in gross overestimation throughout the half-cycle. The logarithmic layer is a consequence of the presence of a constant-stress layer in the boundary layer. It is not surprising that the presence of a fluctuating pressure gradient would disturb this constant-stress layer, as evidently occurs in the second half-cycle. Note that this situation is analogous to the

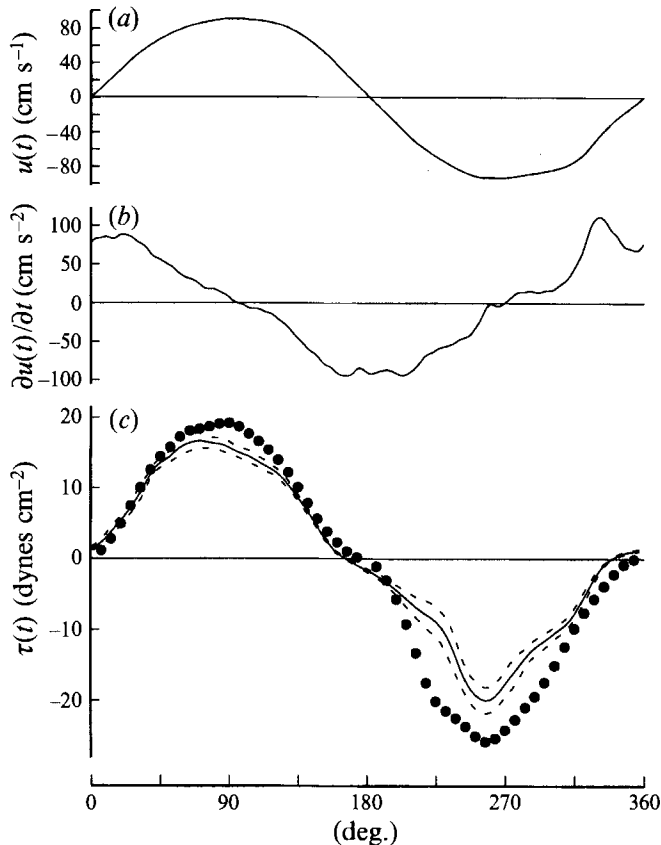


FIGURE 4. Ensemble-averaged time series of (a) centreline velocity, (b) centreline acceleration, and (c) bed stress for the unventilated case. Dashed lines in (c) represent \pm one standard deviation from 15 independent ensemble-averaged estimates of the same quantity. Solid circles are bed-stress estimates from log-layer fit.

steady-current boundary layer subject to waves in which the fluctuating pressure gradient of the waves acts to increase the 'apparent' roughness of the bed (Grant & Madsen 1979). As a consequence of this anomalous behaviour, the following convention is adopted throughout the paper. When discussing bed stress, results from only the first half-cycle are used, and the sense of ventilation will be alternated to provide both suction and injection during that half-cycle. The full cycle will be utilized when presenting velocity and turbulence profiles as these quantities are weakly affected by small fluctuations in the pressure gradient. This can be verified by comparing both half-cycles in the controls runs ($\tilde{V} = 0$). While, in general, the bed-stress results from the second half-cycle differ quantitatively from the first, they are qualitatively the same and the conclusions arrived at in this work are supported by the results from both half-cycles.

In the following subsections the influence of boundary ventilation on oscillating flow will be explored by individually considering the effect on the boundary-layer velocity profile, the turbulent characteristics of the boundary layer and the bed stress. The results presented are primarily for a sinusoidal flow.

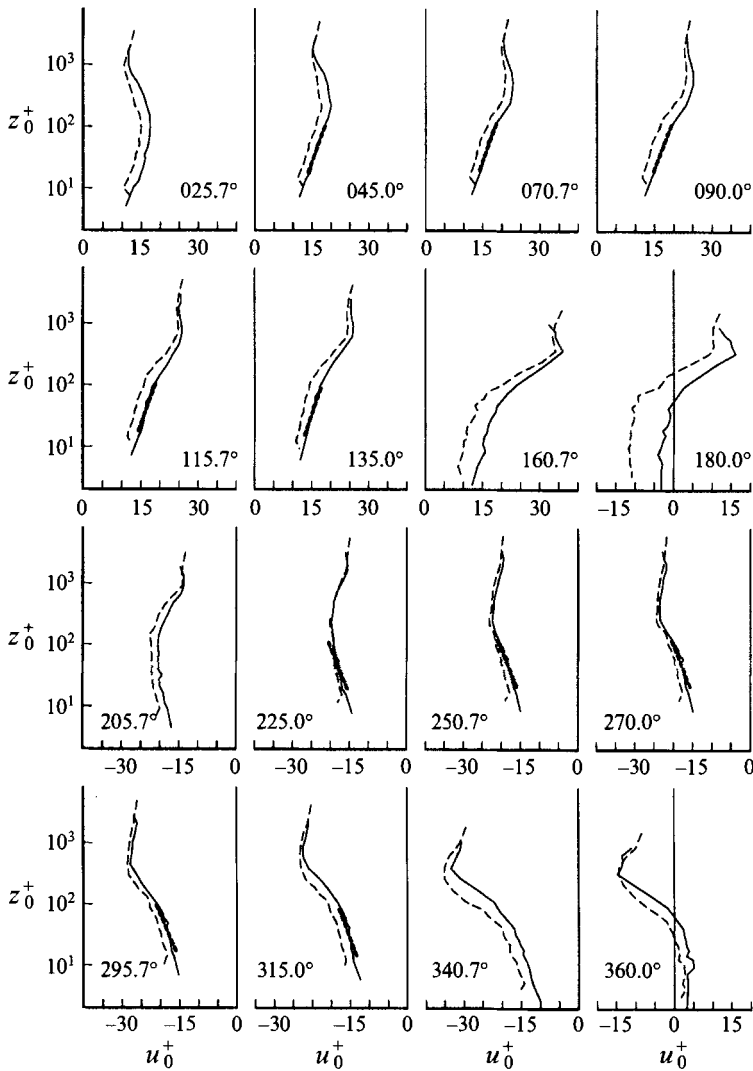


FIGURE 5. Boundary-layer velocity profiles during one cycle. Solid lines are for no ventilation and dashed are for $V = 1.7 \times 10^{-3}$ (injection occurs for $0^\circ < \theta < 180^\circ$). Values of u_* from the unventilated case are used in normalization for both profiles. Heavy dashed lines are the log layers used for computing solid circles in figure 4.

3.1. Boundary-layer velocity

As discussed earlier, the most direct way that suction is expected to affect the boundary layer is to draw the velocity profile down closer to the bed. This results in higher mean velocities near the bed and greater shear at the bed. The effect of injection is expected to be just the reverse, namely streamlines are pushed away from the bed, leading to lower mean boundary-layer velocities and reduced near-bed shear. This is the pattern seen in figure 5, which shows a series of boundary-layer profiles given in semilogarithmic coordinates at various phases throughout one cycle. At each phase there are two profiles. The solid line represents the velocity profile for the case of no ventilation and the dashed line represents the velocity profiles for $\tilde{V} = 1.7 \times 10^{-3}$. The wall variables used in this figure are calculated using u_* from the unventilated case. The

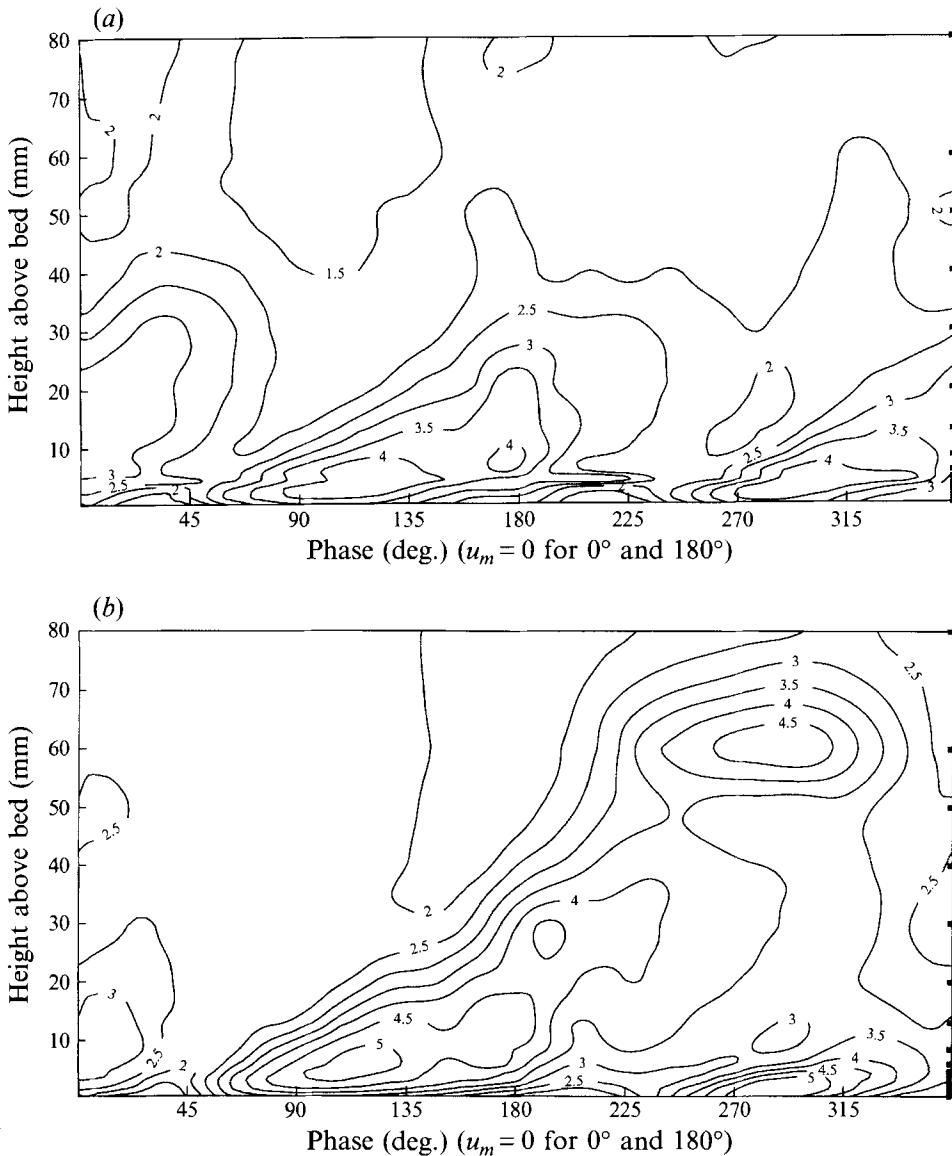


FIGURE 6. Contour plot showing development over height and phase of \bar{w} for (a) unventilated case, (b) for $\bar{V} = 3.3 \times 10^{-3}$. Injection in (b) occurs from 0° to 180° . Contours are in units of $\% u_m$. Boxes on right correspond to measurement locations. Notice relative symmetry between half-cycles in (a).

heavy dashed lines represent the log layer used in the calculations for figure 4. The velocities in the boundary layer are clearly affected even at this level of ventilation. During the occurrence of suction ($180^\circ \leq \theta \leq 360^\circ$) the mean velocities throughout the boundary layer are uniformly greater than the unventilated velocities. This fact necessitates that the vertical velocity gradient at the bed is greater, which is in fact clear in the figure. Once again, just the reverse is true for injection ($0^\circ \leq \theta \leq 180^\circ$). It is even more readily evident that the mean velocities throughout the boundary are lower with injection than for the unventilated case and therefore the near-bed vertical velocity gradient is less than for the unventilated case.

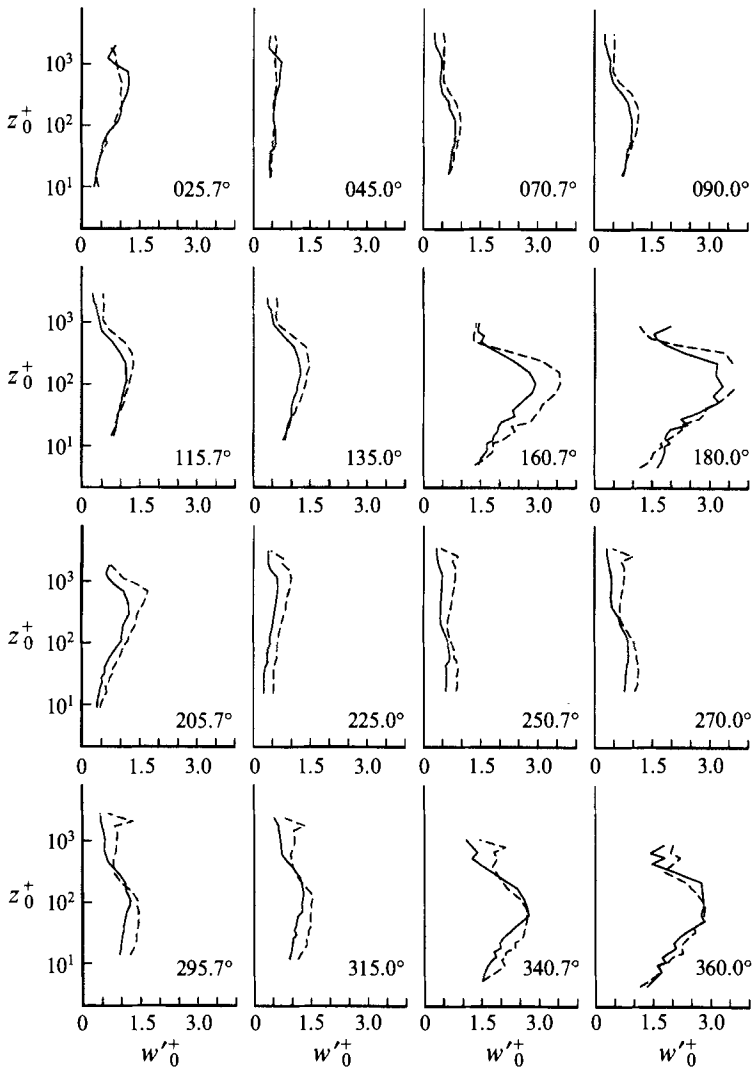


FIGURE 7. Boundary-layer profiles of $\overline{w'}$ during one cycle. Solid lines are for no ventilation and dashed are for $\tilde{V} = 3.3 \times 10^{-3}$ (injection occurs for $0^\circ < \theta < 180^\circ$). Values of u_\star from the unventilated case are used in normalization for both profiles.

Considering the symmetric nature of unventilated oscillatory flow, it is clear that the above observations imply an asymmetry in the mean boundary-layer velocities for a ventilated oscillatory boundary layer. This asymmetry must be realized as a net current in the boundary layer above the permeable bed. This current will be positively directed for negative \tilde{V} and vice versa.

3.2. Turbulence

A contour plot of the development of $\overline{w'}$ over phase and elevation is shown in figure 6(a). This is for the case of no ventilation and the results are qualitatively similar to those reported by others (see Sleath 1987). Sleath (1987) reported that w' and u' behave qualitatively the same, so for the following discussion it will be assumed that the behaviour of w' is indicative of turbulent intensities in general. The maximum in turbulence intensity is seen to occur near the bed just following the start of deceleration

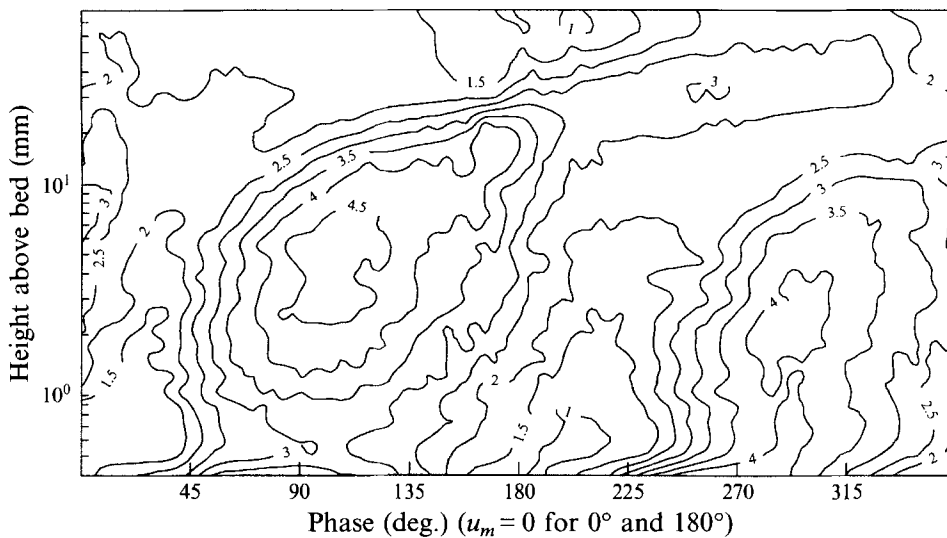


FIGURE 8. Contour plot showing development over height and phase of $(\overline{w'^2})^{1/2}$ for $\tilde{V} = 1.7 \times 10^{-4}$. Contours are in units of $\% u_m$ and height scale is logarithmic. Injection occurs from 0° to 180° . Boxes on right correspond to measurement locations.

(90° and 270°). From this maximum the turbulence slowly diffuses upward over phase giving the impression of an inclined plume. For unventilated oscillatory flow, this pattern is relatively symmetrical with turbulence maxima occurring at about the same level in each half-cycle, and the size, shape and inclination of the turbulent plumes are similar in each case. It is also seen that the turbulence levels associated with each half-cycle return to the background level prior to the arrival of the next plume.

The effects of ventilation on the turbulent properties of the flow are shown in figure 6(b). This is a contour plot of the development of $\overline{w'}$ over phase and elevation for the case of $\tilde{V} = 3.3 \times 10^{-3}$. The figure shows three major effects of ventilation. The first effect is that, near the bed, the turbulence levels are higher with suction ($180^\circ \leq \theta \leq 360^\circ$) than injection. Second, with suction the turbulence maximum is drawn closer to the bed. Finally, owing to the flow stabilizing tendency of suction and the destabilizing influence of injection, the turbulent plumes have become very distorted. In particular, the turbulent plume originating in the half-cycle with suction is very much diminished and is contained in a thin layer (≈ 5 mm) drawn near the bed. The turbulent plume from the injection half-cycle is much enhanced, extending higher into the flow and, consequentially, persisting long into the subsequent half cycle. This tendency is so pronounced that it would appear that the majority of the turbulence that arises from the injection half-cycle occurs during the suction half-cycle. The net effect of this is that a 'snapshot' of turbulence levels at constant phase would show the highest turbulence levels to occur during the half-cycle with suction even though that turbulence develops from unstable flow occurring during the half-cycle with injection. Figure 7 presents the same data in a series of plots at constant phase using the same type of inner scaling as in figure 5.

Using a logarithmic elevation scale, the contour plot of the time history of $\overline{w'}$ (figure 8) shows that the previously described qualitative picture is true for \tilde{V} as low as 1.7×10^{-3} , the lowest ventilation parameter for which data of this type were collected. In short, with suction, the near-bed turbulence levels are enhanced and the associated turbulent plume is confined close to the bed. The turbulent plume associated with

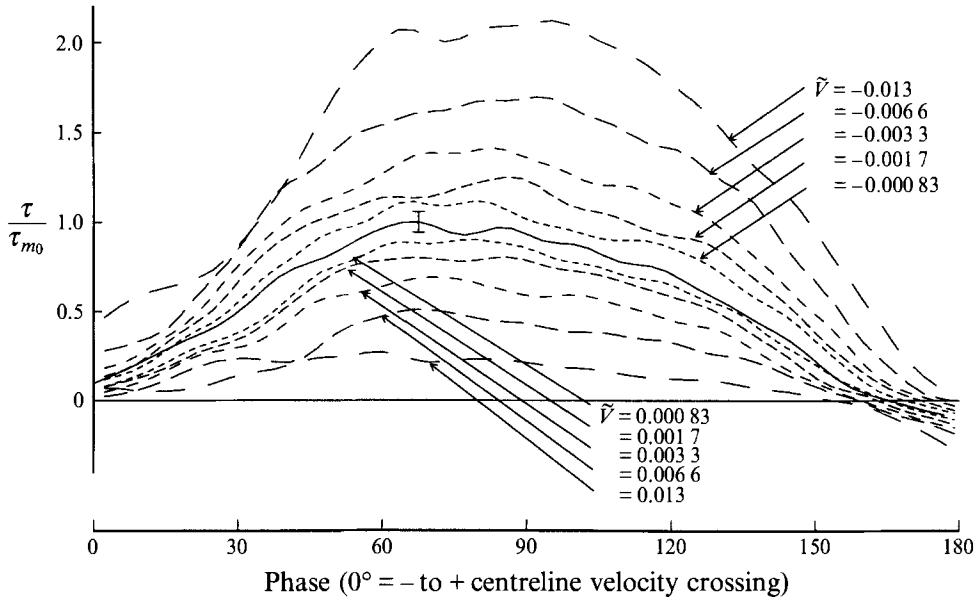


FIGURE 9. Ensemble-averaged bed stress for various values of \tilde{V} . Values are normalized by the maximum unventilated bed stress. Solid line is bed stress for unventilated case. The error bar represents 95% confidence level of peak stress.

injection extends higher into the flow, and persists in time throughout most of the subsequent half-cycle, returning to background levels by the end of the cycle.

3.3. Bed stress

The effect of boundary ventilation on bed stress is summarized in figure 9, in which a full half-cycle of ensemble-averaged bed stress is plotted for various ratios of the ventilation parameter \tilde{V} . The ensembles are calculated from runs of 71 cycles. The solid line is the bed stress for the case of no ventilation and serves as the baseline for the other tests. The peak value from this curve is used to normalize all the data. As seen in the figure, ventilation clearly affects the bed stress throughout the entire cycle in oscillatory flow. As expected, suction ($\tilde{V} < 0$) leads to increased bed stress and injection ($\tilde{V} > 0$) causes reduced bed stress. This figure shows that there is a significant stress reduction or enhancement for ventilation parameters with magnitudes as low as 8.3×10^{-4} .

The data from figure 9 have been used to construct figure 10. For each value of \tilde{V} , the bed stress was integrated over all positive values then divided by the half-period to arrive at a mean bed stress over a half-cycle. These values were normalized by the mean bed stress for no ventilation and plotted as a function of ventilation parameter as represented by the open points in figure 10. If we denote the ratio of mean bed stress ($\langle \tau \rangle / \langle \tau_0 \rangle$) as R_i and consider this ratio as equivalent to the ratio of friction factors in (1), then we can construct an expression similar to (1) for the oscillatory case:

$$R_i = \frac{b\tilde{V}/f_w}{e^{b\tilde{V}/f_w} - 1}, \tag{6}$$

where $f_w = 2\tau_m/\rho u_m^2$ is the wave friction factor (Jonsson 1963). The dashed line in figure 10 represents (6) using the theoretical steady-flow value of 2.0 for b which

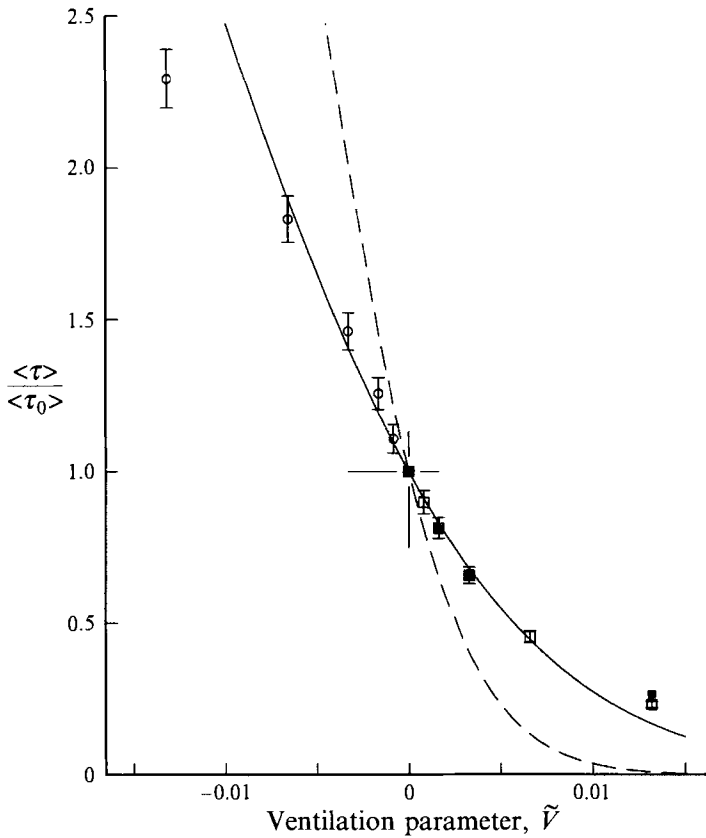


FIGURE 10. Time-averaged ventilated bed stress *vs.* injection parameter \tilde{V} . Values are normalized by time-averaged unventilated bed stress. Averages are for first half-cycle. Error bars represent 95% confidence interval based on repeated estimates of ensemble-averaged quantity. Variance is assumed to be a constant fraction of measurement. Circles are for $\tilde{V} < 0$ and boxes are for $\tilde{V} \geq 0$. Solid boxes represent estimates based on (7) over the bottom 0.01 cm. Solid line is from equation (6) using $b = 0.9$ and dashed line is with $b = 2.0$.

appears to over predict the integrated effects of ventilation for oscillatory flow. The solid line represents (6) using a value of 0.9 for b . This is the mean value arrived at by fitting all the data points to (6) and does a superior job in explaining the observed results, particularly for low values of \tilde{V} .

Even in a turbulent boundary layer, viscous stresses dominate within the viscous sublayer. Mickley *et al.* (1954) have shown that in boundary layers with suction, the boundary-layer velocity in this layer can be expressed as

$$u^+ = \frac{e^{A^+ z^+} - 1}{A^+}, \quad (7)$$

where $A^+ = w/u_*$. Notice that as w goes to 0, the above equation approaches the well-known relation $u^+ = z^+$. It is generally accepted that the viscous sublayer is present for $z^+ \leq 5$ (Schlichting 1979). The lowest elevation for which velocity was measured was at 0.01 cm, which is within the viscous sublayer for all phases. It is therefore possible to calculate a second estimate of bed stress utilizing (7). This process has been carried out using the velocity record at 0.01 cm and the results have been plotted on figure 10

as filled boxes. While in general, the precision of this technique is poor, the results do show good agreement with the shear-stress sensor data and provide one more level of confirmation for these results.

4. Persistence of ventilation effects

It has been shown that the velocity profile, turbulent characteristics and bed stress in an oscillatory boundary layer are highly affected by ventilation when the oscillatory flow is sinusoidal and there is no phase lag between the maximum ventilating flow and the boundary-parallel flow. The sensitivity of these effects to the Reynolds number of the flow, the shape of the oscillations and the phase separation between the two flows will now be investigated. The comparisons will be done by examining the effect on bed stress as this effect is easiest to quantify and contrast.

4.1. \overline{Re} dependence

In order to determine the Reynolds-number dependence of the effects of boundary ventilation, a series of tests were performed in which the flow \overline{Re} was varied. Using the linear relationship between d_0 and u_m , it can be shown that (2) is equivalent to

$$\overline{Re} = d_0^2 \sigma / 4\nu. \quad (8)$$

As all tests were performed using the same frequency, reductions in \overline{Re} were achieved by reducing d_0^2 by the appropriate factor. The range over which \overline{Re} was varied was determined by the limits of the physical apparatus. The largest \overline{Re} (1.0×10^6) represented the largest stroke which could be safely obtained from the hydraulic ram, and the smallest (1.0×10^5) represented the lowest volume of water which could be accurately pumped through the permeable bed at the \tilde{V} value of 3.3×10^{-3} .

Figure 11 shows the results of these tests. At each \overline{Re} the ensemble-averaged mean stress with ventilation has been integrated over one oscillatory half-cycle. These values were then normalized by the integrated bed stress for the unventilated case at the appropriate \overline{Re} . These values have been plotted as the circles and squares in figure 11. The bars on the plots represent 95% confidence intervals. The lines in this plot are calculated from (6) and appear to predict the trend of the data quite well. As can be seen in the figure, \overline{Re} dependence is weak particularly at the higher \overline{Re} values.

4.2. Phase dependence

Since most of the results presented in this paper are for boundary ventilation which is in phase with the free-stream flow, it was decided to test the sensitivity of the flow to variations in the phase relationship between the two flows. Zero phase ($\phi = 0$) in this section is defined as the condition when the maximum magnitude of the boundary ventilation occurs simultaneously with the maximum in the free stream. As used here, positive phase means that maximum ventilation occurs prior to the maximum free-stream velocity, and negative phase therefore implies that maximum ventilation follows the free-stream maximum. The range of phases has been restricted to $\pm 90^\circ$ with separate tests for suction and injection.

It should be noted that any phase difference between the two flows implies that each half-cycle will experience periods of both suction and injection. As this suggests that each half-cycle experiences periods of both increased and reduced bed stress, presenting results in terms of bed stress integrated over a half-cycle would not be appropriate. Instead results are presented in terms of maximum bed stress normalized by maximum unventilated bed stress. These values are presented in figure 12 where open circles

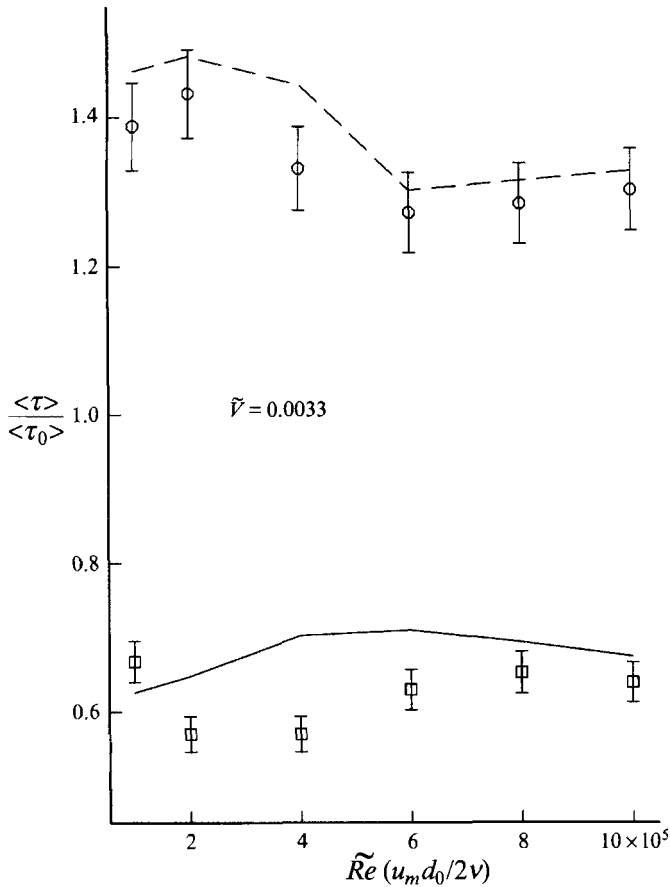


FIGURE 11. Time-averaged ventilated bed stress *vs.* \tilde{Re} . Values are normalized by time-averaged unventilated bed stress. Averages are for one half-cycle. Lines are computed from (6) using $b = 0.9$. Error bars are 95% confidence interval (see figure 10 for discussion of computation).

represent the results for suction and the squares are the values for injection. The error bars represent 95% confidence limits calculated from the variance of the maximum stress measurements.

The lines in figure 12 represent the predicted effect of phase offsets in boundary ventilation if it is assumed that the parameter of importance is the instantaneous ventilation parameter \tilde{V}' . Such an assumption would imply that flow history has no role in the effect of boundary ventilation and that the flow instantly responds to the present conditions. While such an assumption may be unreasonable, these lines aid in determining just what role flow history does play. The instantaneous ventilation parameter for the time of peak velocity can be easily calculated as the cosine of the phase offset times the flow ventilation parameter \tilde{V} . Using these values of \tilde{V}' , the expected stress reduction or enhancement can be predicted from a plot similar to figure 10 which is based on stress maxima rather than integrated stress. This procedure is used in constructing the lines in figure 12.

The principal resemblance between the observed results and those predicted by the above-described 'prevalent condition' hypothesis is that the effect of ventilation is a maximum around a phase offset of 0° and drops off to no effect (ratio = 1) at $\pm 90^\circ$. Ventilation effects are seen not to be a critical function of phase, that is phase

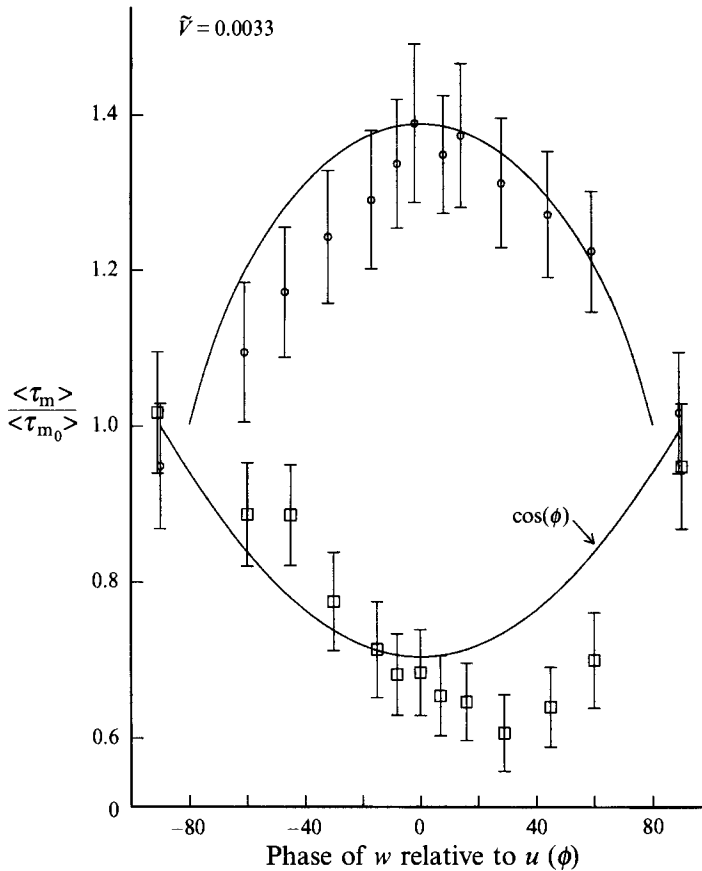


FIGURE 12. Maximum ventilated bed-stress values normalized by maximum unventilated bed stress as a function of ventilation phase ϕ . Open circles are for suction, open boxes are for injection. Solid lines are expected response assuming instantaneous response. Error bars represent 95% confidence interval based on variance of ensemble-averaged estimate.

differences of $\pm 10^\circ$ do not radically change the effects of ventilation. In fact, the changes in bed stress over this range are not statistically different from each other. However, for larger phase differences, the drop off rate is clearly different for each quadrant and therefore warrants inspection in all quadrants. The most straightforward behaviour occurs for boundary suction with positive phase offset. Here the effects of ventilation appear to follow the simple cosine response. This suggests that with a stabilized boundary layer, as exists with suction, the streamlines equilibrate rapidly toward their undisturbed state as the level of applied suction is reduced. While not behaving as smoothly as suction with positive phase, injection with negative phase difference appears to also follow the cosine behaviour. It is important to recall the sequence in the development of the boundary layer for this case. The half-cycle begins with decreasing suction. Eventually the boundary ventilation switches to injection. We have already seen that the boundary layer will quickly respond to the reduction of suction so the tendency for the bed stress to follow the cosine response implies that, when applied to a stable or unventilated boundary layer, the response time for shear reduction due to injection is small with respect to the timescales of the flow.

The behaviour of injection with positive phase offset contrasts strongly with the above descriptions. In fact the only resemblance that the effect of boundary injection

with positive phase difference has to cosine response is that the stress ratio does return to one at 90° . Figure 12 illustrates that stress reduction due to injection grows at phase offsets greater than 0° even though the instantaneous ventilation parameter is decreasing. To understand this behaviour it is important once again to consider the time history of the boundary layer. In this situation, the boundary layer has experienced boundary injection for the entire half-cycle prior to the occurrence of maximum stress. The maximum injection rate occurs prior to the occurrence of maximum stress, which occurs during a time of decreasing injection. With this scenario in mind, it appears that the spreading of boundary-layer streamlines induced by boundary injection is resistant to readjustment. In fact the slight tendency for increased stress reduction with phase suggests that, once a level of spreading is developed, it can be maintained by smaller ventilation flows than originally present. In contrast to compressed boundary layers which appear to readjust immediately to changing conditions, boundary-layer spreading appears to be resistant to readjustment. This result is fully consistent with results for steady flow subject to changing transpiration.

This interpretation seems to be validated by the results for boundary suction with negative phase. In this quadrant, the half-cycle commences with boundary injection leading to boundary-layer spreading. With the onset of suction, the streamlines are indeed drawn closer to the bed leading to greater bed stress for greater suction, but the level of bed stress enhancement never manages to attain the level it does for a boundary layer which was not initially subject to injection.

4.3. Sensitivity to velocity asymmetry

In order to test how sensitive the effects of boundary ventilation are to the shape of the free-stream velocity, a series of experiments were performed with an asymmetrical velocity waveform, a plot of which is shown in figure 13. This waveform was taken from a time series of orbital velocities beneath near-breaking waves in the ocean. This particular wave was chosen because of its strong asymmetry, 7 s period and the similarity of its flow parameters to the oscillatory waveforms generally employed in this study. The peaked form of asymmetry (skewness) for this wave is 0.88 while the sawtooth form of asymmetry has a value of -0.31 (Hasselmann, Munk & MacDonald 1963; Elgar & Guza 1985). The orbital displacement distance d_0 for this form was 182 cm. The maximum orbital velocity was 111 cm s^{-1} . Using (2) this gives $\overline{Re} = 1.0 \times 10^6$.

Exactly the same waveform was used to drive the ventilation velocity as was used to drive free-stream velocity, and no phase difference was imposed. It should be understood that all suction results come from the peaked high-velocity portion of the waveform (crest) and all injection results come from the flat low-velocity portion of the waveform (trough). The integrated bed stress for each subcycle, normalized by the unventilated integrated bed stress for the appropriate subcycle, is plotted as the open symbols in figure 13. The solid curve is the same one plotted in figure 10. Inspection of figures 13 and 10 suggests that the waveform shape has an insignificant effect on the bed-stress ratio during boundary suction. Wave shape does affect the bed-stress ratio during injection, particularly for larger values of \bar{V} . This can be understood from the discussion in the previous section. The flat profile of the low-velocity section results in a longer period where injection increases only slightly so that the magnitude of ventilation is maintained near its maximum value for a significant portion of the subcycle. It is proposed that injection in this case would result in flow streamlines which exhibit a higher mean separation over the course of the longer-duration subcycle than would be expected with a more sinusoidal profile. This would result in greater

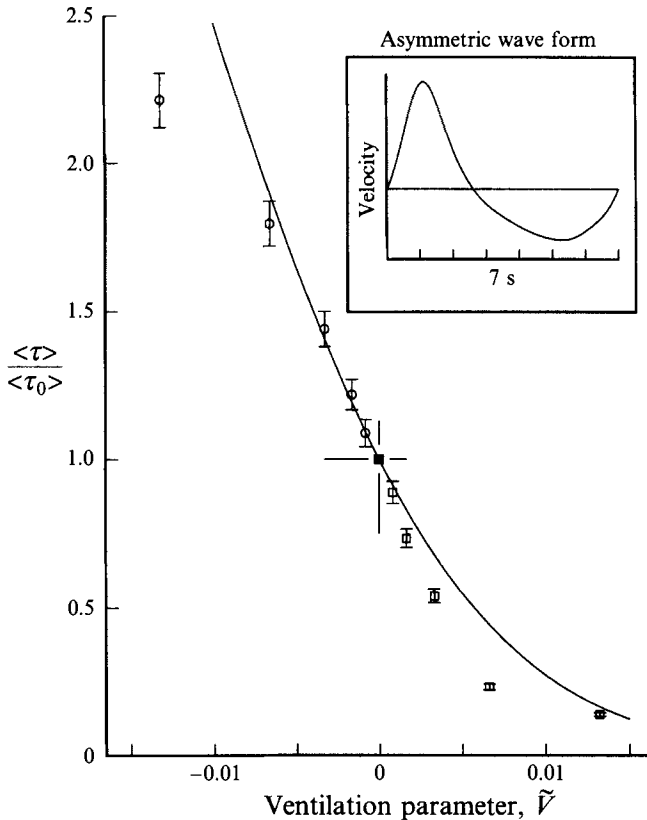


FIGURE 13. Time-averaged ventilated bed stress *vs.* injection parameter \tilde{V} for asymmetric waveform (symbols). The line represents results for a symmetrical waveform (from figure 10). Values are normalized by time-averaged unventilated bed stress. Averages are over one half-cycle. The peaked half-cycle is for $\tilde{V} < 0$ and flat half-cycle for $\tilde{V} > 0$. Error bars represent 95% confidence interval based on repeated estimates of ensemble averaged quantity. Variance is assumed to be a constant fraction of measurement.

bed-stress reduction as is observed in the figure, and consequently greater stress asymmetry.

5. Discussion

The results of these experiments show that the ventilated oscillatory boundary layer exhibits behaviour which could have been qualitatively predicted from knowledge of the manner in which transpiration affects steady boundary layers. The importance of these effects can take on a larger significance in the oscillating case than they would appear to in the steady case because the time average of most quantities in oscillating flows is zero. This can be demonstrated by considering the change in the boundary-layer velocity profile. In an oscillatory boundary layer where the velocities in one half-cycle are just the negative of the velocities in the second half-cycle, the net velocity over one full cycle is identically zero. However, in a ventilated oscillatory boundary layer where suction leads to higher velocities near the bed while injection causes spreading of the velocity profile and lower near-bed velocities, a net velocity occurs in the boundary layer. The sense of this velocity is in the direction of the oscillatory flow which is subject to suction.

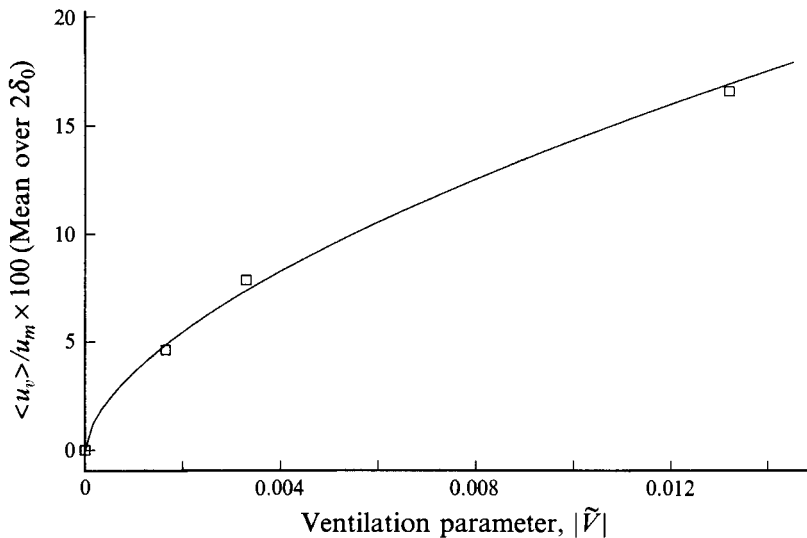


FIGURE 14. Normalized net boundary-layer velocity averaged over a distance $2\delta_0$ (normalized ventilation current) vs. absolute value of \tilde{V} . Net velocity is presented as a percentage of u_m . Line is equation (9). Sign of net velocity is the opposite of the sign of \tilde{V} .

A mean net boundary-layer velocity has been determined for the values of \tilde{V} for which velocity profiles were measured. This was done by integrating the mean velocity profiles over a height of $2\delta_0$ (3.6 cm). This vertically averaged mean velocity was then integrated over an entire cycle to arrive at the mean vertically averaged net velocity herein called the ventilation current $\langle u_v \rangle$. These values have been plotted in figure 14. The line in figure 14 is a least squares fit for the relation $\langle u_v \rangle / u_m = q \tilde{V}^n$. The best fit was found to be

$$\langle u_v \rangle / u_m = 2.27 \times |\tilde{V}|^{0.6}. \quad (9)$$

In this relation, the sign of $\langle u_v \rangle$ is opposite to the sign of \tilde{V} .

Liu (1977) and Sleath (1978) discuss mass transport in progressive water waves propagating over a permeable bed which is essentially a ventilated oscillatory boundary layer. Their analysis, based on laminar-boundary-layer theory, predicts that the permeable boundary and resultant ventilation introduce a component of mass transport in the boundary layer which diminishes the traditional mass transport above a solid boundary. In essence they conclude that ventilation contributes an effective mass transport in the fluid layer which is in the direction of flow experiencing injection. While the present study does not include progressive wave phenomena, the results here, which relate to the distortion of flow streamlines in the boundary layer due to ventilation, indicate a mass transport which enhances the traditional mass transport and consequently is in the opposite direction as well as an order of magnitude larger than that predicted by Liu (1977) and Sleath (1978).

While the bed experiences no net stress in a purely sinusoidal boundary layer, there is a net bed stress with ventilation. This net stress is a consequence of the bed-stress reduction due to injection and the bed-stress enhancement due to suction. When the two half-cycles are averaged together they result in a net bed stress. Figure 15 shows the net bed stress due to a ventilated oscillatory boundary layer as a function of \tilde{V} . The results of figure 9 have been used to construct this plot. The points in figure 15 represent the difference between the integrated bed stress with suction and the integrated bed stress with injection normalized by twice the integrated unventilated bed

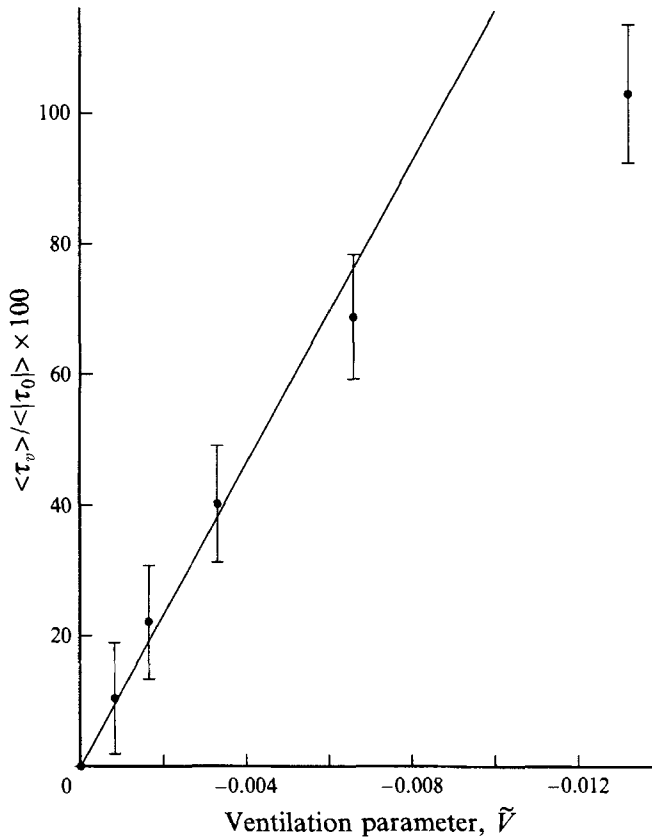


FIGURE 15. Average net ventilated bed stress as a percentage of average gross unventilated bed stress vs. \tilde{V} . Solid line is computed from (10) with $b = 0.9$. Error bars are 95% confidence interval.

stress, where integration is over one half-cycle. These points therefore represent the mean net stress over an entire period as a percentage of the mean gross stress for the unventilated case. Using (6) we can derive the following relation for this quantity:

$$\frac{\langle \tau_v \rangle}{\langle |\tau_0| \rangle} = \frac{b\tilde{V}}{2f_w}. \tag{10}$$

The solid line in figure 15 is this equation using a value of 0.9 for b . The above relation suggests that a 1% net stress is obtained with a ventilation parameter as small as 9×10^{-5} ! It should again be observed that this net stress is in the direction of the oscillating flow experiencing suction.

It is worthwhile to consider the importance these results may hold for geophysical situations. Reid & Kajiura (1957) and others have shown analytically that a gravity wave travelling through a fluid medium over a permeable bed will induce boundary ventilation. It can be shown that for geophysically reasonable permeabilities, the ventilation parameter \tilde{V} will not exceed 1×10^{-3} and that phase differences between u and w will be $O(5^\circ)$ or less. This suggests that in general wave-driven ventilated boundary layers will produce a mean boundary current in the direction of wave advance and with a magnitude which can be determined through a knowledge of \tilde{V} . A net stress in the direction of wave advance will be induced, with a magnitude which can be predicted by (10). These phenomena will be relatively \overline{Re} independent over an order

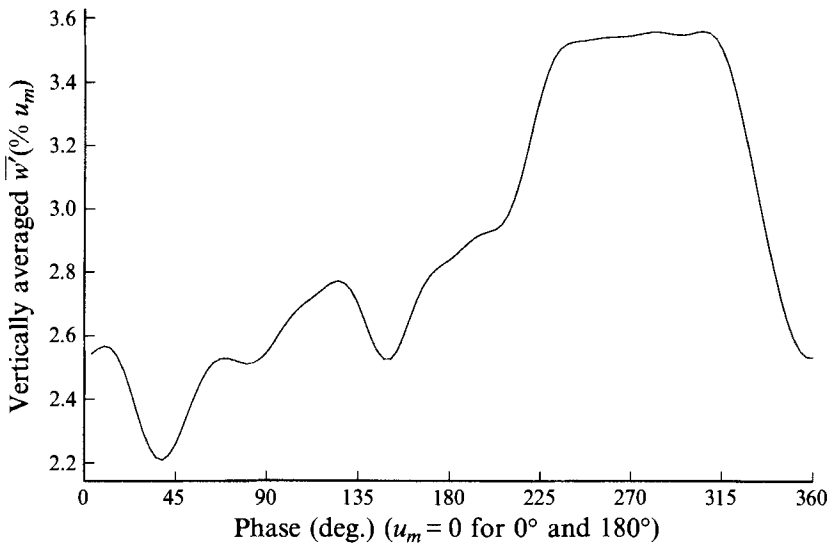


FIGURE 16. Vertically averaged turbulence (\bar{w}) level as a function of wave phase θ . Average is over 8 cm and $\bar{V} = 3.3 \times 10^{-3}$.

of magnitude of \bar{Re} as shown in figure 11. Over the expected range of phase separation between the wave potential flow and boundary ventilation, phase would not be expected to significantly alter these results. While gravity waves are not expected to exhibit a sinusoidal profile and will develop inherent asymmetries, the results of figure 13 indicate that for low values of \bar{V} the flow will still exhibit the behaviour discussed above.

This study shows that ventilated oscillatory boundary layers will develop net boundary velocity as well as net bed stress even in the absence of any other asymmetry. This result has obvious implications for studies of transport in such flows. The implications of the asymmetry in turbulence are not so easy to predict. Figure 6(b) shows quite clearly that the majority of the turbulence throughout the cycle originates from the injection half-cycle. Yet how this would affect the transport of some quantity is far from clear. If sediment transport is approximated by the product of suspension and local velocity and the level of suspension is proportional to the instantaneous turbulence levels, the argument can be made that transport would once again be in the direction of flow during suction. This can be understood by examining figure 16, which gives a time history of the vertically averaged turbulence levels present in figure 6(b). This figure, which imparts no information about history, clearly shows that the maximum vertically averaged turbulence levels occur during the suction half-cycle. By the above assumptions, transport due to turbulent suspension would be in the direction of flow during suction, even in the absence of other asymmetries. As suspended transport under waves is a more complicated phenomenon than simple instantaneous averages, the above scenario may be wholly inaccurate. However, it does help to demonstrate the possible ramifications that these findings have for suspended transport.

6. Conclusions

A laboratory experiment was performed to test the effect of boundary ventilation on the mean velocities, turbulent flow characteristics and bed stresses in an oscillatory boundary layer. The results of these experiments lead to the following conclusions.

(i) Boundary suction causes flow streamlines to be pulled toward the bed, leading to higher velocities near the bed, whereas injection leads to streamline spreading and reduced near-bed velocities. This effect results in a mean near-bed flow with sign opposite to that of the ventilation parameter.

(ii) The enhanced velocity shear near the bed during suction results in increased bed stress while the reduced shear during injection results in diminished bed stress.

(iii) The above effects which are observed to be strong functions of the ventilation parameter \tilde{V} can be well predicted by (6). The bed stress is shown to be essentially independent of \bar{Re} for the range of \bar{Re} tested. It is also shown that phase dependence is small for small phase differences between u and w . The effects of suction are insensitive to waveform shape while the effects of injection increased with increasing length of the injection subcycle. These wave shape modifications were negligible for small values of \tilde{V} .

(iv) Boundary ventilation leads to a strong asymmetry in flow turbulence. Enhanced turbulent fluctuations are maintained in a thin layer near the bed with suction and turbulent diffusion is reduced. Away from the bed turbulence levels are enhanced by injection leading to greater turbulent diffusion initiated during injection. The result of these effects is enhanced vertically averaged turbulence levels during suction.

This study was funded by the office of Naval Research, Coastal Sciences under grant N00014-89-J-1060 with the University of California, San Diego. We are indebted to Robert Guza for his insightful comments and suggestions throughout the experiments. Aid in instrumentation and facilities preparation was provided by Charles Coughran, John Powell, Mike Kirk and Domingo Goyena and others at the Scripps Institution of Oceanography hydraulics laboratory. The comments of the anonymous referees were thoughtful and appreciated.

REFERENCES

- ANTONIA, R. A., BISSET, D. K., FULACHIER, L. & ANSELMET, F. 1990 Effect of wall suction on bursting in a turbulent boundary layer. *Phys. Fluids A* **2**, 1241–1247.
- ANTONIA, R. A., FULACHIER, L., KRISHNAMOORTHY, L. V., BENABID, T. & ANSELMET, F. 1988 Influence of wall suction on the organized motion in a turbulent boundary layer. *J. Fluid Mech.* **190**, 217–240.
- BLINCO, P. H. & SANDBORN, V. A. 1975 Use of the split-film sensor to measure turbulence in water near a wall. In *Turbulence in Liquids* (ed. G. K. Patterson & J. L. Zakin), pp. 403–413. Dept. Chemical Engineering, University of Missouri-Rolla.
- CONLEY, D. C. & INMAN, D. L. 1992 Field observations of the fluid-granular boundary layer under near-breaking waves. *J. Geophys. Res.* **97** (C6), 9631–9643.
- ELGAR, S. & GUZA, R. T. 1985 Observation of bispectra of shoaling surface gravity waves. *J. Fluid Mech.* **161**, 425–448.
- FLICK, R. E. & GEORGE, R. A. 1990 Turbulence scales in the surf and swash. *Proc. 22nd Conf. on Coastal Engng*, pp. 557–569. ASCE.
- FLICK, R. E., GUZA, R. T. & INMAN, D. L. 1981 Elevation and velocity measurements of laboratory shoaling waves. *J. Geophys. Res.* **86** (C5), 4149–4160.
- FULACHIER, L., ELENA, M., VEROLLET, E. & DUMAS, R. 1982 Suction effects on the structure of turbulent boundary layer on a heated porous wall. In *Structure of Turbulence in Heat and Mass Transfer* (ed. Z. P. Zorac), pp. 193–220. Hemisphere.
- GRANT, W. D. & MADSEN, O. S. 1979 Combined wave and current interaction with a rough bottom. *J. Geophys. Res.* **84** (C4), 1797–1808.
- HANES, D. M. & HUNTLEY, D. A. 1986 Continuous measurements of suspended sand concentration in a wave dominated nearshore environment. *Cont. Shelf Res.* **6**, 585–596.

- HASSELMANN, K., MUNK, W. & MACDONALD, G. 1963 Bispectra of Ocean waves. In *Time Series Analysis* (ed. M. Rosenblatt), pp. 125–139. John Wiley.
- JENSEN, B. L., SUMER, B. M. & FREDSOE, J. 1989 Turbulent oscillatory boundary layers at high Reynolds numbers. *J. Fluid Mech.* **206**, 265–297.
- JONSSON, I. G. 1963 Measurements in the turbulent wave boundary layer. *Proc. 10th Congr. IAHR*, pp. 85–92.
- JUSTESEN, P. 1987 Turbulent wave boundary layers. *Series Paper 43*. Inst. Hydrodyn. and Hydraul. Eng., Tech. Univ. of Denmark, Lyngby.
- KAYS, W. M. 1972 Heat transfer to the transpired turbulent boundary layer. *Intl J. Heat Mass Transfer* **15**, 1023–1044.
- KING, D. B., POWELL, J. D. & SEYMOUR, R. J. 1984 A new oscillatory flow tunnel for use in sediment transport experiments. *Proc. 19th Conf. Coastal Engng*, pp. 1559–1570. ASCE.
- LIBBY, P. A., KAUFMAN, L. & HARRINGTON, R. P. 1952 An experimental investigation of the isothermal laminar boundary layer on a porous flat plate. *J. Aero. Sci.* **X**, 127–134.
- LIU, P. L.-F. 1977 Mass transport in water waves propagated over a permeable bed. *Coastal Engng* **1**, 79–96.
- LOFQUIST, K. E. B. 1975 An effect of permeability on sand transport by waves. *Tech. Memo. 62*. US Army Corps of Engrs, Coastal Engng Res. Center.
- MICKLEY, H. S. & DAVIS, R. S. 1957 Momentum transfer for flow over a flat plate with blowing. *Tech. Note 4017*. Natl Adv. Comm. Aeronaut., Washington.
- MICKLEY, H. S., ROSS, R. C., SQUYERS, A. L. & STEWART, W. E. 1954 Heat, mass, and momentum transfer over a flat plate with blowing or suction. *Tech. Note 3208*. Natl Adv. Comm. Aeronaut., Washington.
- REID, R. O. & KAJIURA, K. 1957 On the damping of gravity waves over a permeable sea bed. *EOS, Trans. AGU* **38**, 662–666.
- SCHLICHTING, H. 1979 *Boundary Layer Theory*, 7th edn. McGraw-Hill.
- SIMPSON, R. L., MOFFAT, R. J. & KAYS, W. M. 1969 The turbulent boundary layer on a porous plate: Experimental skin friction with variable injection and suction. *Intl J. Heat Mass Transfer* **12**, 771–789.
- SLEATH, J. F. A. 1978 Mass transport in water waves propagated over a permeable bed (Liu, 1977). *Coastal Engng* **2**, 169–171.
- SLEATH, J. F. A. 1987 Turbulent oscillatory flow over rough beds. *J. Fluid Mech.* **182**, 369–409.
- TEWFIK, O. E. 1963 Some characteristics of the turbulent boundary layer with air injection. *AIAA J.* **1**, 1306–1312.